Particle size distributions in the upper 100 m water column and their implications for animal feeding in the plankton

George A. Jackson [a,*], David M. Checkley Jr [b]

[a] Department of Oceanography, Texas A&M University, College Station, TX 77843, USA
[b] Scripps Institution of Oceanography, University of California, San Diego, La Jolla, CA 92093, USA

ARTICLE INFO

ABSTRACT

We deployed autonomous particle-sensing SOLOPC floats more than eight times during five cruises, amassing almost 400 profiles of particle size ($d > 90$ μm) and abundance between the ocean surface and 100 m. The profiles consistently had subsurface maxima in particle volume. The median (by volume) equivalent spherical diameter for the particle distribution was 0.4–0.8 mm and increased with depth in a manner similar to that observed in coagulation simulations. There was a sharp cutoff at the bottom of the high particle concentration region. Estimation of particle fluxes made using the size distributions show an increasing downward movement through the particle field above the sharp particle cutoff. The increase of particle flux with depth through the euphotic zone implies a partial spatial separation of production and consumption. The sharp drop in particle volume and flux implies that the base of the particle-rich zone is a region of active particle consumption, possibly by zooplankton flux feeding. Our data show greater concentrations of zooplankton-type particles relative to marine snow-type particles below the particle maximum. Such behavior could explain why zooplankton are frequently observed at and immediately below the particle maximum rather than the productivity maximum and suggests an important role for flux feeding in carbon and nutrient cycling at the base of the particle maximum. This implies that zooplankton act as gatekeepers for the movement of organic matter to the mesopelagic. The ability of the SOLOPC to sample hourly with high resolution in the upper 100 m of the ocean provides a powerful complement for the study of particles where it has been difficult to use sediment traps.

© 2011 Elsevier Ltd. All rights reserved.

1. Introduction

A dominant goal of biological oceanography during the last two decades has been to understand the factors that control the fate of organic matter in the ocean. The particulate nature of marine organisms has profound implications for how they find each other, how they grow and die, and how they sink. Dominant processes that affect particle concentrations include growth, coagulation, consumption, and settling. Size is an important particle property controlling all of these processes.

While the euphotic zone is the source of organic matter for the deep ocean, all the problems associated with the direct measurement of flux using sediment traps are accentuated there (e.g., Buesseler et al., 2007). Indirect measurements provide insight into the processes around the euphotic zone. For example, Buesseler et al. (2005, 2008) made fine-scale measurements of [234]Th distributions near the ocean surface to infer the sources and sinks of falling organic matter. Typically they found a relative deficiency in [234]Th in the euphotic zone caused by the adsorption to and subsequent settling loss of organic matter from it. Buesseler et al. (2008) observed regions of enhanced [234]Th activity at the base of the euphotic zone, which they ascribed to the capture, consumption, and remineralization of falling particles by zooplankton. Again, localized interaction of zooplankton and falling particles was invoked to explain these observations.

Particles have been counted and measured directly near the surface using in situ imaging techniques (e.g., Walsh and Gardner, 1992, Lampitt et al. 1993a,b, MacIntyre et al., 1995; Stemmann et al., 2000). Invariably, there is a maximum in particles near the base of the surface mixed layer. This maximum has been associated with turbulent processes (MacIntyre et al., 1995) and with zooplankton feeding (e.g., Lampitt et al., 1993b).

Gehlen et al. (2006) tested various biogeochemical models to determine the fate of organic matter leaving the near-surface and how it influenced the deep ocean. They argued that aggregation processes that alter the particle size distribution and, hence, the particle flux, are essential "to initiate an intense biological pump."

* Corresponding author. Tel.: +1 979 845 0405.
E-mail addresses: gjackson@tamu.edu (G.A. Jackson),
dcheckley@ucsd.edu (D.M. Checkley Jr).

Table 1
Particulars of SOLOPC deployments. t_0 is deployment time, hours local time; lat_0 and $long_0$ are the latitude and longitude at deployment; z_{max} is the maximum sampling depth.

Cruise	deploy #	ID	launch d	t_0	lat_0	$long_0$	# prof	z_{max}(m)
Sproul 05	1	sp05	28-Sep-05	0906	33.01° N	−118.01°	63	100
New Horizon 06	1	nh06	14-Sep-06	1701	34.28	−121.14	86	100
Sproul 07	1	sp07_1	23-Mar-07	2024	34.77	−117.56	9	100
	2	sp07_2	23-Mar-07	1738	32.78	−117.55	12	100
Thompson 07	1	th07_1	4-Apr-07	0821	34.26	−120.88	70	100
	2	th07_2	9-Apr-07	1744	33.62	−123.09	72	100
	4	th07_4	16-Apr-07	0205	34.20	−121.16	76	100
Knorr 08	1	bl08	2-May-08	2020	61.15	−25.37	10	150

They also noted that "Below the wind mixed layer, POC fluxes are most sensitive to the intensity of zooplankton community composition." Their analysis highlights the importance of both aggregation and zooplankton grazing to the vertical flux for the euphotic zone.

We have developed and deployed the autonomous SOLOPC float to measure the concentrations of particles, including aggregates and zooplankton, in the upper 100–150 m of the water column (Checkley et al., 2008). We have deployed SOLOPC floats more than eight times during four cruises off Southern California and one in the North Atlantic (Table 1). We now have almost 400 profiles of particle size and abundance in the ocean surface layer.

The conditions of our deployments ranged from eutrophic to oligotrophic and from near-coastal to open ocean. Four of the deployments (sp05, nh06, and sp07_1 and sp07_2) were described in Checkley et al. (2008). Three of the deployments (th07_1, th07_2, and th07_4) occurred during the CCE LTER process cruise on the R/V Thompson, which was described in Landry et al. (2009). The final deployment (bl08) occurred at the start of a cruise of the R/V Knorr to study the North Atlantic Bloom.

In this paper we use our results from the SOLOPC to calculate particle abundance as a function of depth and particle size. We also use particle properties to infer particle type (aggregates and zooplankton) and how these relate to other water properties at multiple locations. We use spectra of particle abundance to estimate the fluxes of different size classes throughout the upper water column, assuming a size-dependent sinking rate.

We present a detailed set of results for one deployment, th07_1, in an upwelling region off Point Conception, California (Table 1). This deployment had the highest particle volume that we observed. We then compare observations among all of our deployments. Lastly, we discuss the implications for the particle flux and its control by animals.

2. Methods

2.1. The SOLOPC float

The SOLOPC is an autonomous biological profiler which combines a Sounding Oceanographic Lagrangian Observer (SOLO) float, reporting vertical profiles of temperature, salinity, and depth, with a Laser Optical Plankton Counter (LOPC) and a WET Labs ECO Puck. We used either a fluorescence or a backscatter ECO Puck sensor for each deployment. The LOPC senses individual plankters and other particles over a size range of 0.09–35 mm as they pass through a sheet formed by 70 adjacent 1 mm × 1 mm beams of red (640 nm) light (Herman et al., 2004). The particle-sensing region has a cross-sectional area of 49 cm² and thickness of 1 mm. For a 100 m vertical profile, the total volume sampled for particles is 0.49 m³. The SOLOPC has been described in detail by Checkley et al. (2008).

2.2. Data collection

The LOPC handles small and large particles differently. Small particles (single-element particles, SEPs) are detected by the attenuation of one or two light beams as objects pass through the light field. Each SEP is assigned an equivalent spherical diameter (d_{esd}) and a count is added to the appropriate d_{esd} bin. The number of counts in the size bins is saved every 3 s, equivalent to about a 60 cm depth interval. Larger particles (multiple-element particles, MEPs) intercept more than two light beams; for each beam, maximum light attenuation and duration is recorded. We designate the width of the beams they intercept as the occluded diameter (d_{od}). In our data analysis, we calculated the d_{esd} from the total light attenuation for each MEP (Checkley et al., 2008) and added this count to the appropriate d_{esd} bin to create a size-frequency distribution for all (SEP+MEP) particles observed by the LOPC in each time interval. (Note that symbols are defined in Table 2.)

2.3. Data interpretation

2.3.1. Particle type

MEPs, particles with $d_{od} > 2000$ μm, are composed of at least two types, relatively opaque animals and relatively amorphous and transparent aggregates, distinguished by their ratios of d_{esd} to d_{od}. The relationships used to calculate d_{esd} were determined using opaque spheres and, thus, d_{esd} is closer to the mass-equivalent diameter than is d_{od}. Aggregates tend to have much larger values of d_{od} than d_{esd} because of their amorphous natures (e.g., Jackson et al., 1997). We calculated the number of MEPs for bins of each 1 mm d_{od} increment and 0.1 mm d_{esd} increment. That is, we calculated a two dimensional histogram for size distributions using d_{od} and d_{esd} for each MEP. We determined the mean d_{esd} value ($\hat{d}_{esd}$) for the $\hat{d}_{esd}$ bin having the largest number of particles for each d_{od} bin value. We fit a curve of the form

$$\ln\hat{d}_{esd} = \alpha + \beta\ln d_{od} \tag{1}$$

If all particles were opaque, β would be 1; β decreases with increasing transparency of particles. This is equivalent to fitting

$$\left(\frac{\hat{d}_{esd}}{\hat{d}}\right)^3 = \left(\frac{d_{od}}{\hat{d}}\right)^f \tag{2}$$

where $f = 3\beta$ is the fractal dimension and $\hat{d} = e^{\alpha/(1-f/3)}$ is a scaling constant, which can be interpreted as the diameter of a single source particle, i.e., where $\hat{d}_{esd}$ equals d_{od}. Thus, f is maximal (3) for opaque particles and decreases with increasing transparency of particles.

We used Eq. (1) to calculate $\hat{d}_{esd}$ and classify MEPs as either z-particles (zooplankton) or s-particles (marine snow). MEPS with $d_{esd} > 2\hat{d}_{esd}$ were classified as z-particles; particles with

Table 2
Notation. All volumes based on d_{esd}. $1\,\mu M = 1\,nmol\,cm^{-3} = 1\,mmol\,m^{-3}$.

Symbol	Meaning	Typical units
B	Particle mass concentration in volume of water	$g\,cm^{-3}$
d	Particle diameter	cm
d_{esd}	Particle equivalent spherical diameter	cm
d_{od}	Particle occluded diameter	cm
$\hat{d}$	Parameter in fractal relationship	cm
$\hat{d}_{esd}$	Estimate of d_{esd} made using d_{od} and fractal scaling	cm
f	Fractal dimension	–
F	Particle carbon vertical flux	$gC\,m^{-2}\,d^{-1}$
g	Gravitational acceleration	$cm^2\,s^{-1}$
m	Particle mass	
n_d	Differential number spectrum, in terms of d	cm^{-4}
ρ	Particle density	$g\,cm^{-3}$
$N(s)$	Number concentration of particles larger than size s	cm^{-3}
V	Volume of an individual particle	cm^3
$V_{int}(d)$	Integrated volume of particles smaller than d	–
V_{sep}	Integrated volume of sep particles in a volume of water	–
V_{sno}	Integrated volume of s-particles in a volume of water	–
V_{zoo}	Integrated volume of s-particles in a volume of water	–
V_{tot}	Total particulate volume in a volume of water	–
α, β	Curve fit parameters	
v	Fluid viscosity	$cm^2\,s^{-1}$
ρ_C	Carbon density of particles	$g\text{-}C\,cm^{-3}$
ρ_f	Fluid density	$g\,cm^{-3}$
$\Delta\rho$	Difference between particle and fluid densities	$g\,cm^{-3}$

$d_{esd} \leq 2\hat{d}_{esd}$ were classified as s-particles. Unless otherwise indicated, particle diameter d in subsequent calculations refers to d_{esd}.

2.3.2. Particle number and volume spectra

Particle counts within a depth range of 5 m were summed and sorted into logarithmic size bands, with the d_{esd} of the upper value of a band equal to 1.1447 times the lower. Thus, the volume of a particle at the upper bound of a band is 50% greater $(1.1447^3 = 1.5)$ than the volume of a particle at the lower bound. Using a logarithmic binning scheme allows the bin width to increase with particle size and thus increases the number of particles per bin for larger particles, for which there are frequently too few particles to register in small, fixed-width bins.

The cumulative number spectrum $N(d)$ is the number of particles larger than d; we use the subscript j to denote the jth depth range. The particle number spectrum n_{ij} for the ith bin and jth depth range was estimated by dividing the number of particles within the size range of the ith bin (ΔN_{ij}) by the sample volume and the d_{esd} range for the bin (Δd_i). The volume spectrum nV was calculated by multiplying n_{ij} by $\pi d_i^3/6$, the volume of a particle with a d_{esd} equal to the median d_{esd} for the bin, d_i. We calculated spectra for SEPs, z-particles, and s-particles, as well as for all particles considered together.

The distribution of particle volume is given by the volume spectrum nV, with the area under the curve proportional to the total volume when nV is plotted as a function of d. Plotting nV against the logarithm of d shows more detail in the distribution for smaller d but loses the relationship between area under the curve and total particle volume. The curve area-particle volume equivalence is restored when plotting the normalized volume spectrum nVd as a function of the logarithm of diameter. The nVd spectrum is a convenient way of displaying the particle volume distribution over a large size range without losing the relationship between the area under the curve and the integrated particle volume.

The resulting spectra for one such cruise, nh06, spanned d_{esd} from 106 μm to 0.54 cm in 30 bins, where the diameters of the spectral values are the average of upper and lower d_{esd} bounds for the bins. Each spectrum was matched with the mean chl a

fluorescence, measured using the fluorescence sensor and expressed as a digitized voltage, for its 5-m depth interval within its profile. A comparison of 18 chlorophyll concentrations measured from samples collected in bottles with the equivalent fluorescent signal provided a linear relationship of chl $a(\mu g\,L^{-1}) = -0.4428 + 0.003313 \times$ the voltage signal ($r^2 = 0.83$).

The volumetric concentration of particles for $0.01\,cm < d < d_{max}$ was determined by integrating the volume spectrum numerically:

$$V_{int}(d_{max}) = \int_{0.01cm}^{d_{max}} nV\,\mathrm{d}d \tag{3}$$

The total particle volume V_{tot} was calculated as $V_{int}(0.54\,cm)$, the maximum observed particle diameter.

The cumulative number spectrum for a given d was calculated by numerical integration of the number spectrum from the largest particle size to d:

$$N(d) = \int_d^{d_{max}} n\,\mathrm{d}d \tag{4}$$

Particle concentrations are frequently presented as number concentration larger than 0.5 mm (e.g., MacIntyre et al., 1995), equivalent to $N(0.5\,mm)$.

The water column density and Brunt–Väisälä frequency N_{BV} were calculated from the measured temperature, salinity and depth using subroutines in the Oceans Toolbox for Matlab (available at acoustics.whoi.edu/pub/Matlab/oceans/).

2.3.3. Particle flux

The particle flux $F\,(gC\,m^{-2}\,d^{-1})$ was calculated by multiplying the mass spectrum nm by the particle settling speed v_s and numerically integrating over the size range:

$$F = \int_{0.01\,cm}^{0.54\,cm} nmv_s\,\mathrm{d}d \tag{5}$$

where m is the carbon content of a particle with diameter d (e.g., Guidi et al., 2007).

Particle mass m was estimated as

$$m = \rho_C V \tag{6}$$

where $\rho_C = 0.067\ \text{gC cm}^{-3}$ is the carbon-to-volume ratio for phytoplankton (Mullin et al., 1966). The settling velocity was estimated as (Jackson, 1995)

$$v_s = \frac{1}{18} \frac{\Delta \rho g}{\rho_f v} \frac{d_{esd}^3}{d_{od}} \qquad (7)$$

where $\rho_f = 1.0275\ \text{g cm}^{-3}$ is the fluid density, $\Delta \rho = 0.01\ \text{g cm}^{-3}$ is the assumed particle excess density, $g = 980\ \text{cm s}^{-2}$ is gravitational acceleration, and $v = 0.01\ \text{cm}^2\ \text{s}^{-1}$ is the fluid viscosity. With these values of m and v_s, F can be calculated using Eq. (5).

The median diameter for the normalized volume spectrum, as calculated here, is the diameter for which $V_{int}(d)/V_{tot} = 0.5$. That is, half the total particle volume is smaller than the median diameter.

Mean values for a deployment were calculated by averaging values over all the dives in a deployment.

3. Results

3.1. General descriptions of the deployments

The general properties of the environment for the deployments are listed in Table 3 and described in greater detail below.

sp05 Deployment sp05 was in Autumn 2005 in the Southern California Bight (SCB) midway between San Clemente Island and San Diego. The water column was relatively warm and stratified, with the sharpest density gradient ~ 20–40 m. Irradiance was not measured but the chl a fluorescence distribution (Checkley et al., 2008) is consistent with a euphotic zone depth (Z_{euph}) ~ 60 m. Conditions appeared to be of intermediate trophic status, based on the relatively warm temperature, low chl a fluorescence, location, and float trajectory (Checkley et al., 2008).

nh06 Deployment nh06 was in Autumn 2006 60 km SW of Pt. Conception, a major upwelling center (Checkley et al., 2008; Checkley and Barth, 2009). The water column was relatively cool and had a shallow mixed layer of variable depth (~ 15–40 m) below which there was a strong thermocline. Irradiance was not measured; we estimated $Z_{euph} \sim 30$–50 musing the vertical distribution of chl a fluorescence (Checkley et al., 2008). Conditions appeared to be eutrophic, based on cool water, high chl a fluorescence, and southerly float trajectory, downstream from Pt. Conception upwelling center.

sp07 Deployments sp07_1 and sp07_2 were in Spring 2007 30 km W of San Diego. The water column was cool with a pycnocline ~ 25–55 m and a thin chl a fluorescence maximum (2.5 µg L^{-1}) ~ 25–40 m. Conditions appeared to be of intermediate trophic status, based on the moderate chl a fluorescence, location, and trajectory (Checkley et al., 2008).

th07 Deployments th07_1, th07_2, and th07_4 were in Spring 2007 southwest of Pt Conception (Landry et al., 2009). Deployment th07_1 began 39 km southwest of Pt Conception in eutrophic waters characteristic of coastal upwelling, with $Z_{euph} \sim 50$ m. Deployment th07_2 began 255 km southwest of Pt Conception in oligotrophic waters characteristic of the California Current, with $Z_{euph} \sim 90$ m. Deployment th07_4 began 63 km southwest of Pt Conception in eutrophic waters characteristic of coastal upwelling, with $Z_{euph} \sim 50$ m.

bl08 Deployment bl08 was in Spring 2008 220 km south of Iceland before the bloom. The water column was cool, with a surface mixed layer to 40–60 m and a thermocline at 80–100 m. Conditions were eutrophic.

To illustrate results from a single deployment, we first present a detailed analysis of results from th07_1. We then present data from all deployments.

3.2. Detailed analysis of th07_1, a deployment in an upwelling region

3.2.1. Relationship between different measures of particle diameter

There was a wide range of d_{esd} for any given d_{od} (Fig. 1). For some particles, the two size estimates were nearly the same. However, most particles had much smaller values of d_{esd}. The d_{esd} with the largest number of particles formed a lobe. The data were fit using Eqs. (1) and (2) to determine a fractal relationship. The relationship between d_{esd} and d_{od} for th07_1 implies $f = 1.8$ and $\hat{d} = 13.3\ \mu\text{m}$.

3.2.2. Average particle distributions as a function of d_{esd} and depth

The average particle distribution, expressed here as the nVd spectrum, was similar to that described in Checkley et al. (2008). There was a well-defined particle abundance maximum, as a function of both particle size and depth, centered between 20 and 40 m (Fig. 2A). Total particle volume decreased sharply below it. The average particle diameter generally increased with depth, ranging from 0.5 to 0.9 mm (see further discussion below). There were particles larger than 1 mm which were not part of the smaller particle structure but which could contain a large fraction of the total particle volume at a given depth. The variability associated with these larger particles was substantial (Fig. 2B), and was associated with uncertainties in determining the mean using the small number of counts sampled. Note that in an nVd spectrum, larger particles have a much greater contribution to the total than their numbers would indicate because multiplying n by Vd ($\sim d^4$) results in a 2 mm particle being weighted 10,000 times more than a 0.2 mm particle.

The size distributions of SEPs and s-particles were similar and both were clearly distinct from those of the z-particles during th07_1,

Table 3
Environmental characteristics of deployments. SCB is Southern California Bight. Depth of euphotic zone (Z_{euph}) estimated from chl a distribution for sp05, nh06, and sp07, as irradiance was not measured; values of th07 from Landry et al. (2009). Temperature (T), salinity (S), and chl a fluorescence at 5 m (mean). Trophic status is a qualitative assessment of trophic status.

| ID	Comments	Z_{euph} (m)	T (°C)	S	chl a(µg L^{-1})	Trophic status
sp05	Inner SCB	60	20	33.5	n/a	Intermediate
nh06	S of Pt Conception	30-50	15	33.2–33.7	3.4	Eutrophic
sp07_1	Inner SCB	50	15	33.7	0.2	Intermediate
sp07_2	Inner SCB	50	15	33.7	0.3	Intermediate
th07_1	SW of Pt Conception	50	12	33.7	2.2	Eutrophic
th07_2	California Current	90	14	33.2	0.2	Oligotrophic
th07_4	S of Pt Conception	50	12	33.7	1.1	Eutrophic
bl08	S of Iceland	n/a	9	35.3	3.0	Eutrophic
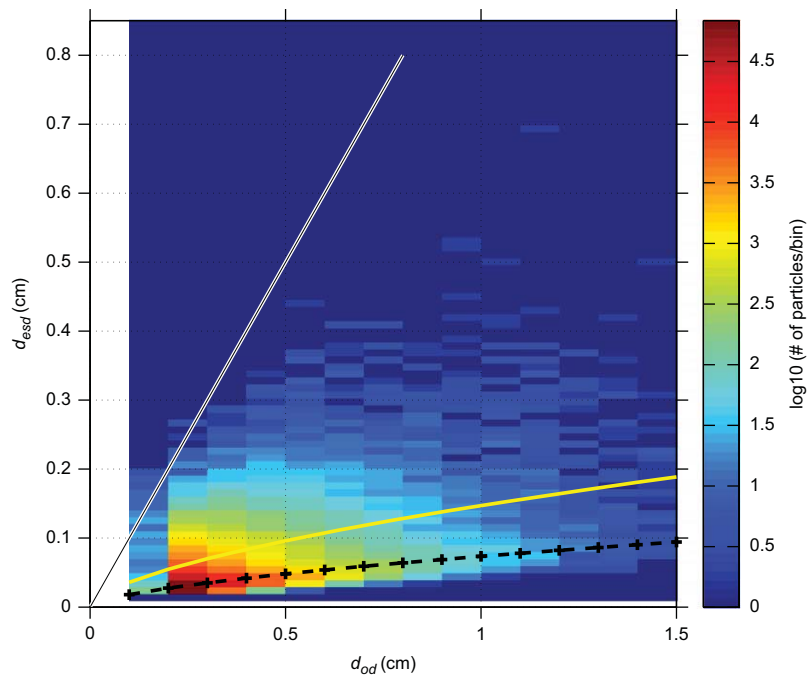
Fig. 1. Relationship between d_{esd} and d_{od} for th07_1. The white line indicates that $d_{esd} = d_{od}$; the dashed black line indicates the fit to the d_{esd} with the maximum number of particles for each d_{od}. Particles with d_{esd} larger than 2 times the value of this line were considered z-particles while those with smaller ESD were considered s-particles. The solid yellow line marks the boundary between the two particle types. The relationship was equivalent to $f = 1.8$ and $\beta = 0.6$. (For interpretation of the references to color in this figure legend, the reader is referred to the web version of this article.)
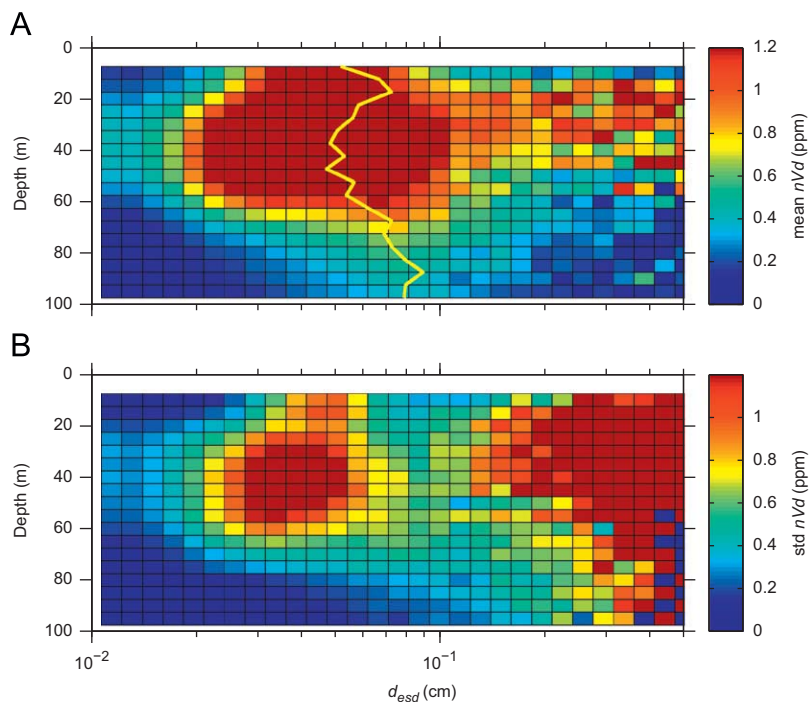
Fig. 2. Mean (A) and standard deviation (B) of the normalized volume distribution nVd for th07_1 deployment. The yellow line in A represents the mean particle diameter. The presence of a few very large particles, possibly zooplankton, around 20 m affects the mean diameter there.

despite the fact that s-particles and z-particles were in the same detection size range (*i.e.*, with similar d_{od}) (Fig. 3). The correlation between V_{sno} and V_{sep} was much greater ($r = 0.79$) than for V_{zoo} and V_{sep} ($r = 0.28$) or V_{zoo} and V_{sno} ($r = 0.43$). The total particle volume, computed from d_{esd}, was similar for the SEP and z-particle fractions during th07_1, though with much smaller amounts in s-particles (Fig. 3). The vertical distributions for total z-particle and s-particle volumes were similar in the upper 60 m, but the s-particles were significantly less abundant deeper (Fig. 4). Despite their smaller volumetric abundances, the s-particles were numerically more abundant, by about a factor of 10, than the z-particles (Fig. 5).

When the particle distributions were expressed as a cumulative number spectrum, N increased by more than four orders of magnitude over the range of particle sizes, from less than
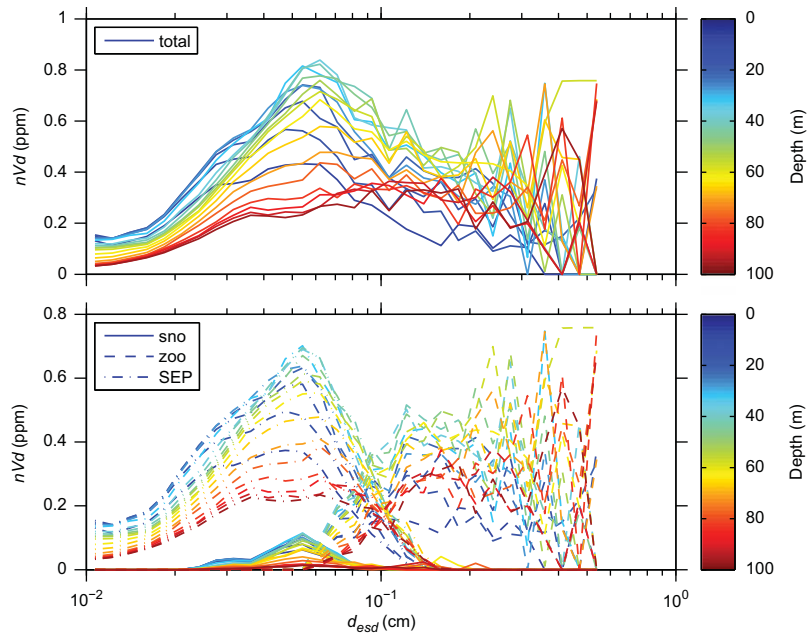
Fig. 3. Volume distribution for different particle classes. Top: total nVd for th07_1. Bottom: nVd of s-particles (-), z-particles (–), and SEPs (-.). Color bar indicates depth associated with line colors. (For interpretation of the references to color in this figure legend, the reader is referred to the web version of this article.)
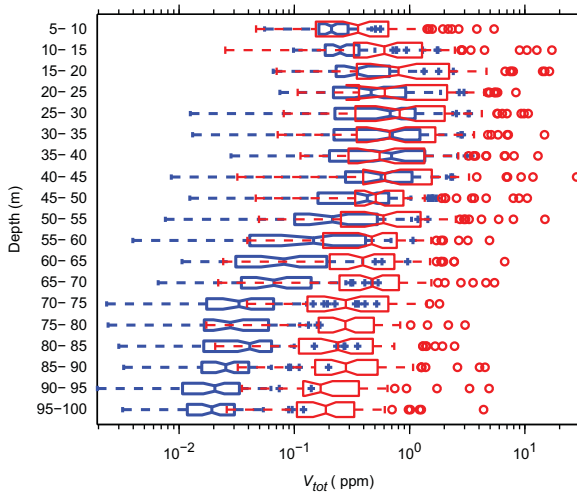

Fig. 4. Distribution of MEP volume with depth for th07_1 deployment. Particles were sorted into z-particle(red) and s-particle (blue). Data for each group are represented as box plots, where the central mark is the median, the edges of the boxes represent the 25th and 75th percentiles, error bars indicate the outermost non-outlier points, and the + symbols indicates outliers. If the notched regions of their boxes do not overlap, two medians are significantly different at the 95% significance level, for normally distributed data. (For interpretation of the references to color in this figure legend, the reader is referred to the web version of this article.)

10^{-2} L^{-1}($d_{esd} \geq 3$ mm) to more than 10^2 L^{-1} ($d_{esd} \geq 100$ μm) (Fig. 6). For comparison with MacIntyre et al. (1995) (see below), $N(0.5$ mm$) = 1.9 - 12.2$ L^{-1}. Using the fractal dimension conversion constants determined below, we calculate that $d_{esd} = 0.5$ mm is equivalent to $d_{od} = 5.2$ mm. If the size assigned to a particle by an imaging system is d_{od} (Jackson et al., 1997), we expect that $N(d_{od} = 0.5$ mm$) = N(d_{esd} = 0.12$ mm$) = 19 - 254$ L^{-1}.

3.2.3. Variability in time, depth

The total particle volume (V_{tot}) varied with depth and time (Fig. 7B). There were particle maxima at about $t = 6.75$ and 7.75 d (6 PM local time) that might be associated with daily production

cycles and/or vertical migration, but the record is not long enough to be definitive. The maximum in N^2_{BV} was below the particle volume maximum about half the time (Fig. 7A, Table 4). The depth of maximum V_{tot} was shallower than that of maximum fluorescence on only 1 of 56 profiles (Fig. 7C).

3.2.4. Correlations with water properties

The correlation between N^2_{BV} and particle volume V_{tot} was weak ($r = 0.38$), as was that between N^2_{BV} and fluorescence ($r = 0.29$; Table 5). The correlation was much greater between V_{sep} and fluorescence ($r = 0.81$) and V_{tot} and fluorescence (Fig. 8, $r = 0.69$). Fluorescence was more highly correlated with V_{sno} ($r = 0.66$) than with V_{zoo} ($r = 0.22$).

3.3. Depth distributions of average water properties for all deployments

3.3.1. Relationship between d_{esd} and d_{od}

The distributions of particles numbers as functions of d_{esd} and d_{od} were similar for all deployments (not shown). Values of f varied from 1.3 to 2.1 for the different deployments and were inversely related to $\hat{d}$. The largest values of f (i.e., more opaque particles) were from deployments with large concentrations of particles (Table 6).

3.3.2. Distribution of particle volume

The pattern of average depth distribution of total particle volume was similar for all cruises (Fig. 9). V_{tot} was low near the surface, reached a maximum between 15 and 70 m depth, and decreased deeper. The decline in V_{tot} was relatively small for the deployments with the smallest maximum particle volume – sp07_1, sp07_2, and th07_2 – for which the maximum time-averaged V_{tot} as a function of depth was less than 1 ppm. The largest average V_{tot} was 5.3 ppm during th07_1; the depth range of this peak was relatively wide, with V_{tot} greater than 5 ppm for a 20 m range. The decrease with increasing depth was relatively rapid, with V_{tot} decreasing by half within 15 m.
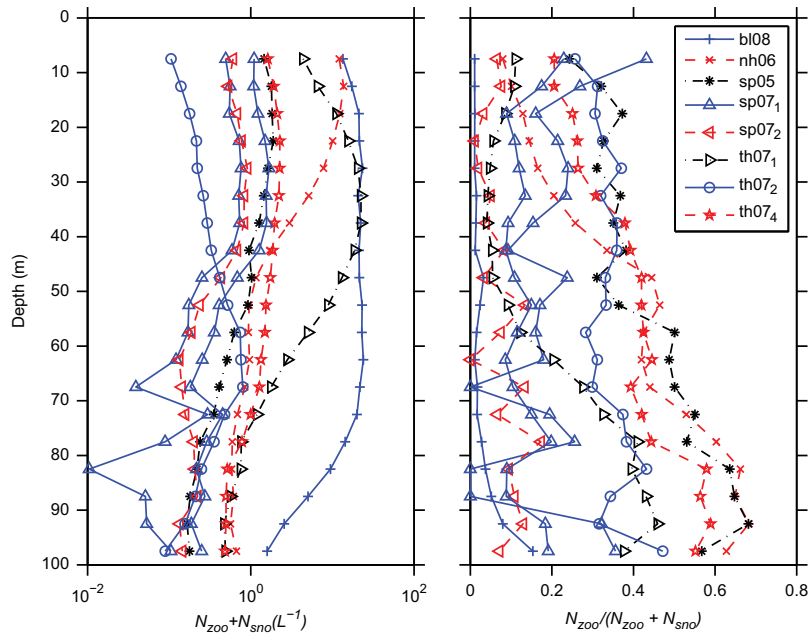
Fig. 5. Depth distribution of total number concentration for all meps (left), and ratio of z-particles to total MEPs (right) for all profiler deployments. Deployments sp07_1 and sp07_1 are essentially replicates of each other.
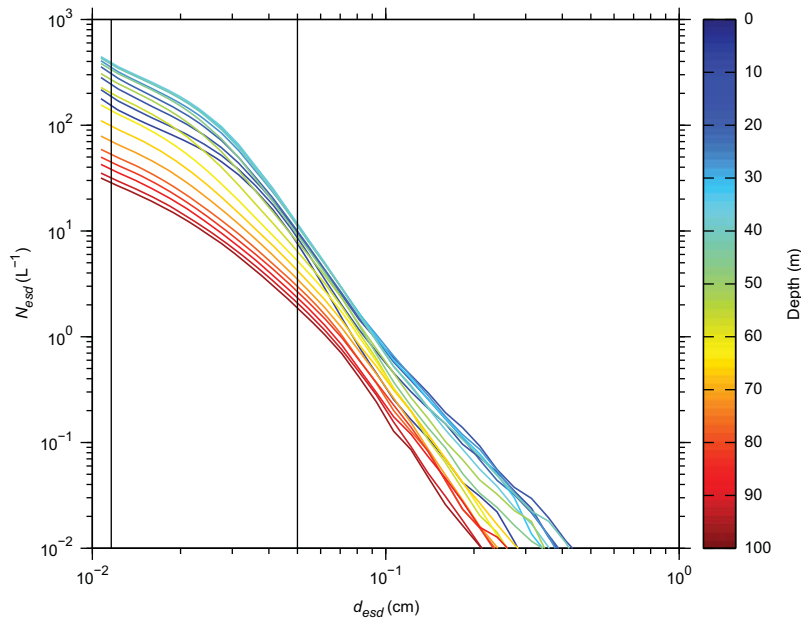

Fig. 6. Cumulative number concentration N as a function of particle diameter for th07_1. Each line represents the average at the same depth over all the dives. The two vertical lines indicate the number concentration of particles that would be observed for particle cutoff $d_{esd} = 0.05$ and 0.116 cm (the second value equivalent to $d_{od} = 0.05$ cm). Color bar indicates depth(m) associated with line colors. (For interpretation of the references to color in this figure legend, the reader is referred to the web version of this article.)

When the particles were classified as s-particles and z-particles, the V_{sno} was smaller than V_{zoo} for all cruises except for the North Atlantic bl08 (Fig. 10). All deployments showed evidence of a subsurface volume max in V_{sno}, although it was minimal for th07_2. Maximum V_{sno} during th07_2 was only 0.2 ppm, small compared to the high concentration of 2.3 ppm for th07_1.

3.3.3. Increase in median particle diameter with depth

The mean particle diameter increased with depth (Fig. 11). The size range for the different deployments was relatively small near the surface, ranging from 250 to 600 μm, but increased so that it ranged from 400 μm to almost 2 mm at 100 m. The mean diameter

was positively correlated with depth for all deployments ($p < 0.05$, mean Kendall's $\tau = 0.73$), except for th07_1, in which there was a slight decrease in particle size at depth ($\tau = -0.15$, $p \sim 0.05$).

3.4. Correlations with water properties

The correlations between V_{sno} and V_{sep}, with $r = 0.51$–0.87 (Table 5), were higher than between V_{zoo} and V_{sep} and between V_{zoo} and V_{sno}. The values of other correlations differed among cruises, but the pattern of low correlation with N_{BV}^2 was similar to that for th07 (Table 5). The correlation between N_{BV}^2 and V_{tot} was as high as $r = 0.77$ during sp05 and as low as 0.02 during bl08.
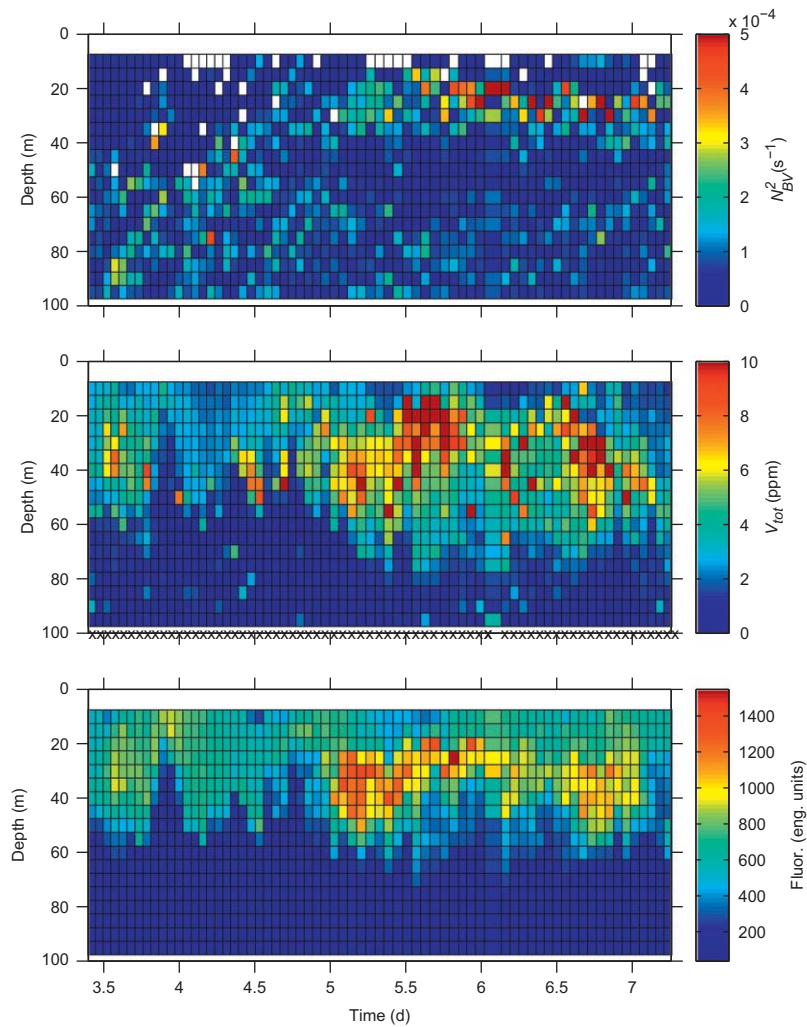
Fig. 7. N_{BV}^2 (proportional to density gradient) (top), V_{tot} (middle) and fluorescence (bottom) for the th07_1 deployment. Particle volume is expressed in ppm, the fractional volume occupied by particles times 10^6. The x marks at 100 m in the middle panel represent the times for which data were collected. Times are given in days, with 5.0 representing midnight and 5.5 being noon.

Table 4
Depth of maximum particle volume V_{tot} relative to depth of maximum density gradient (A,B,C) and fluorescence maximum(D,E,F). Columns present the number of dives where the maximum density was shallower (A), the same (B), or deeper (C) than the maximum V_{tot} or where the fluorescence maximum was shallower (D), the same (E), or deeper (F) than the maximum V_{tot}.

Deploy	N_{BV}^2			Fluorescence		
	shal. A	same B	deep. C	shal. D	same E	deep. F
sp05	43	10	10			
nh06	9	4	73	52	17	1
th07_1	27	7	36	41	14	15
th07_2	11	6	55	22	12	38
th07_4	26	6	44	56	7	13
sp07_1	1	0	8	2	1	6
sp07_2	5	0	7	3	3	6
bl08	4	1	5			

The depths of maximum density gradient N_{BV}^2 and maximum V_{tot} were rarely the same, with maximum V_{tot} being deeper than maximum N_{BV}^2 29%, equal 7%, and shallower 65% of the dives (Table 4). That is, the particle maximum was above the pycnocline more than half the time. Compared to the depth of the maximum fluorescence, maximum V_{tot} was deeper 58%, equal 27%, and shallower 15% of the dives.

3.5. Daily cycles of depth-averaged water properties

Diurnal variations in biological properties are well-known, ranging from changes in zooplankton concentrations to changes in aggregate abundances. We integrated V_{sno} and V_{zoo}, as well as the fluorescence, between 5 and 100 m depth and examined their variations through the day. Only five of the eight deployments (sp05, nh06, th07_1, th07_2, and th07_3) had enough profiles to allow us to analyze for cycles. Of these, only two showed clear evidence of daily cycles in the integrated V_{sno} (sp05, th07_4) and only one in integrated V_{zoo} (Fig. 12). There were no clear cycles in the depth-integrated fluorescence.

For th07_4, the s-particle concentration was greatest in the early evening (18–21 h), with a median of 6.2 cm^3 m^{-2}, and lowest at the end of the night, between 3 and 6 h, with a median of 2.8 cm^3 m^{-2}, and the ratio of the two being 2.2 (*cf*., Checkley et al., 2008). For z-particles, the largest median was also in the early evening 18–21 h, at 81 cm^3 m^{-2}, and the lowest just before noon, at 34 cm^3 m^{-2}, a ratio of high to low of 2.4.

Table 5

Correlation coefficients between fluorescence (fl), total particle volume (V_{tot}) and N_{BV}^2 for different deployments. Also shown are correlations among fluorescence, V_{tot}, V_{sep}, V_{zoo}, and V_{sno} (Fig. 1). The SOLOPC float during sp05 and bl08 did not have a fluorescence sensor.

| Deploy	r N_{BV}^2, V_{tot}	r N_{BV}^2, fl	r fl, V_{tot}	r fl, V_{zoo}	r fl, V_{sno}	r fl, V_{sep}	r V_{sno}, V_{sep}	r V_{zoo}, V_{sno}	r V_{zoo}, V_{sep}
sp05	0.77	–	–	–	–	–	0.58	0.21	0.28
nh06	0.04	−0.17	0.53	0.12	0.72	0.83	0.87	0.26	0.30
sp07_1	0.38	0.29	0.69	0.22	0.66	0.81	0.56	0.26	0.37
sp07_2	0.26	0.12	0.43	0.06	0.39	0.79	0.61	0.48	0.25
th07_1	0.17	0.11	0.69	0.35	0.75	0.77	0.79	0.43	0.28
th07_2	−0.43	0.11	0.46	0.22	0.42	0.74	0.52	0.18	0.19
th07_4	−0.18	−0.30	0.31	0.08	0.56	0.65	0.51	0.27	0.13
bl08	0.02	–	–	–	–	–	0.77	0.13	0.17
Mean	0.13	0.03	0.52	0.18	0.58	0.77	0.65	0.28	0.25
SD	0.36	0.22	0.15	0.11	0.15	0.06	0.14	0.12	0.08
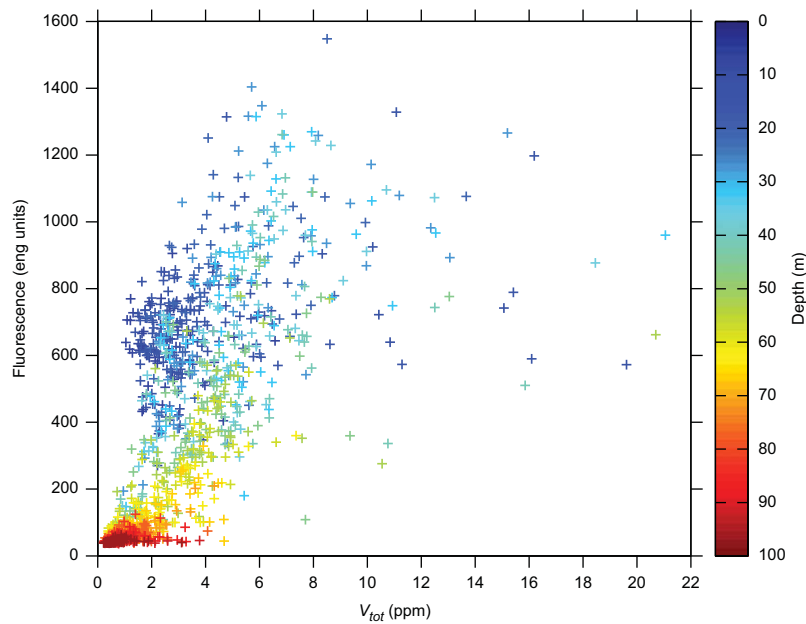
Fig. 8. Relationships between total particle volume and fluorescence signal for a representative cruise, th07_1. The value of $r = 0.69$. The symbol color represents sample depth, with the scale given by the color bar to the right. (For interpretation of the references to color in this figure legend, the reader is referred to the web version of this article.)

Table 6

Fractal dimension and initial particle size inferred from fitting ESD and OD data. Also shown is the largest V_{tot} for the curves shown in Fig. 9. There were too few particles for sp07_1 and sp07_2 to be able to determine the parameters.

Deploy	f	$\hat{d}$ (μm)	max V_{tot} (ppm)
sp05	1.30	66	2.00
nh06	1.56	32	4.74
th07_1	1.80	13	5.26
th07_2	1.39	49	0.74
th07_4	1.67	16	1.79
sp07_1	–	–	0.89
sp07_2	–	–	0.89
bl08	2.09	2.6	3.32

3.6. Change in particle flux with depth

The estimated vertical distribution of particle flux F (Fig. 13) was similar to the distribution of V_{sno} (Fig. 9), but there were important differences (in addition to the abcissa, which is linear in one case and logarithmic in the other). Most dramatic was the sharper decrease in F at the base of the particle maximum. For example, F for th07_1 dropped from almost 0.9 g C m^{-2} d^{-1}
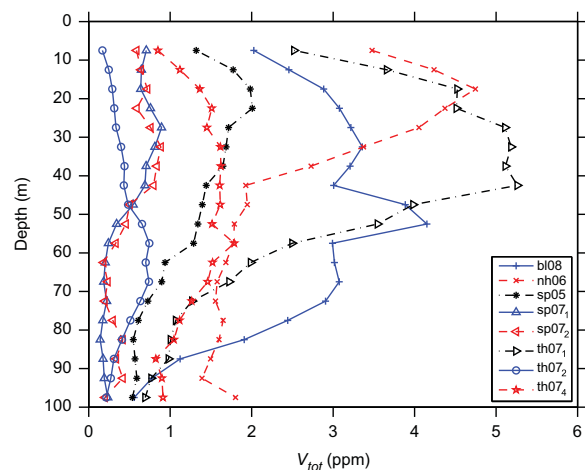

Fig. 9. Depth distribution of time-averaged total volume concentration for all profiler deployments. Deployments sp07_1 and sp07_1 are essentially replicates of each other.

at 40 m to half that value by 50 m. The largest value of F was for the bl08 deployment, 1.1 g C m^{-2} d^{-1} at 73 m. It also had a sharp drop, becoming half that by 80 m. The smallest peak flux was for
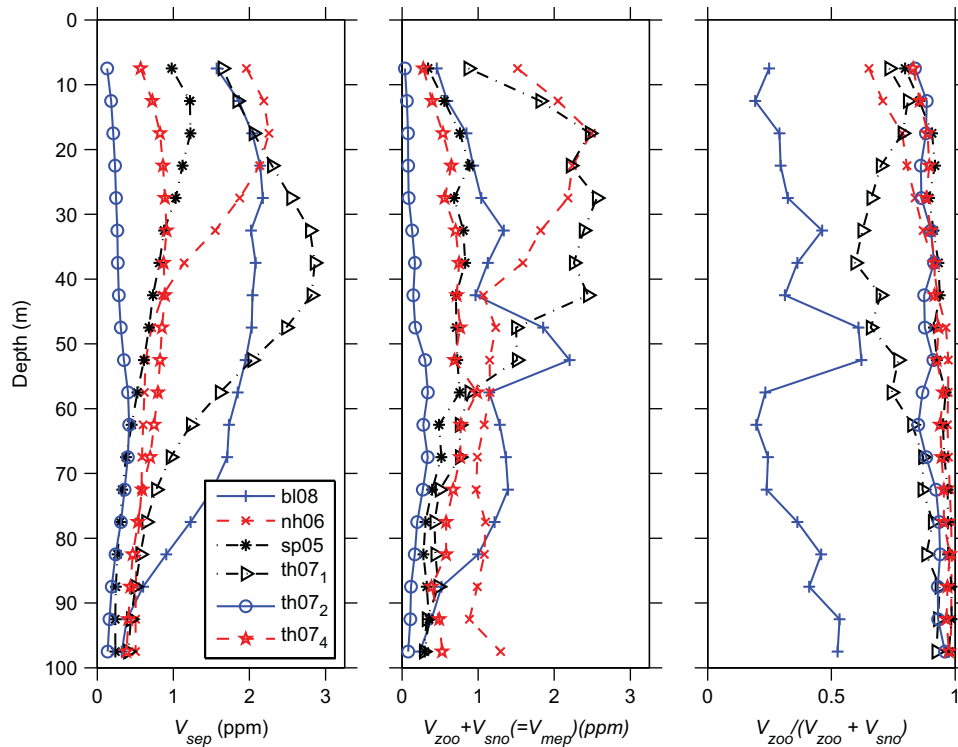
Fig. 10. Depth distribution of particle volume in SEPs (right) and MEPs(center), and the fraction of MEPs that V_{zoo} represents (right).
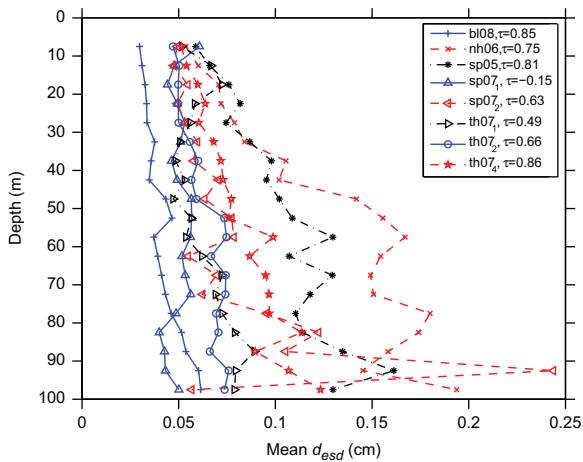

Fig. 11. Mean diameter as a function of depth for multiple deployments. Also shown in the legend are the values of Kendall's τ for the correlation between mean diameter and depth. All correlations except for that of sp07_1 were significant at the 0.05 level.

the oligotrophic station th07_2, less than 0.04 g C m^{-2} d^{-1}. The flux was related to $V_{tot}^{1.6}$. (Pearsons correlation for the log transformed data was $\rho = 0.89$ where the data points were the time-average of values for a depth and cruise. Data from sp07 were not included because of the lack of reliable estimates for f).

4. Discussion

4.1. Particle measurement with the SOLOPC

Researchers have used optical instruments to determine concentrations of zooplankton and marine snow, two quite different types of particles. The multiple measurements made by the LOPC on particles with d_{od} larger than 1 mm allows these particles

to be classified. We were able to separate MEPs into two types with different environmental distributions: s-particles and z-particles.

The z-particles are large and relatively opaque. Because of their similarity in size and opacity to particles previously associated with copepods (Checkley et al., 2008), we consider them to be zooplankton. The s-particles are more transparent; their size and opacity are consistent with their being aggregates (Jackson et al., 1997). For this reason, we consider them to be marine snow particles. Compared to the z-particles, they are numerically more abundant but have significantly lower conserved volumes.

The average fraction of $V_{zoo}/(V_{zoo} + V_{sno})$ for a deployment was $75 \pm 21\%$ for all the deployments. For a similar calculation comparing the numbers, $N_{zoo}/(N_{zoo} + N_{sno}) = 20 \pm 14\%$. Gonzalez-Quiros and Checkley (2006) compared the characteristics of animals captured in net samples to those sampled by an Optical Plankton Counter (OPC) operating *in situ*. They found that a large fraction of the particles observed by the OPC were not found in the plankton samples. They concluded that the OPC was observing large amounts of fragile, marine snow-type, particles that were not surviving the collection process. Their observations about the relative concentrations of these types of particles are consistent with ours.

The volumetric abundance of marine snow particles (V_{sno}) was highly correlated with that of the smaller particles (V_{sep}) measured as SEPs, suggesting that they are similar in composition and are both predominantly aggregates. The fact that both SEPs and s-particles also correlate most highly with the fluorescence values is consistent with their formation by aggregation of algae (*e.g.*, Trent et al., 1978; Alldredge and Gotschalk, 1988).

4.2. Comparison with previous measurements of marine snow abundance

Most *in situ* surveys of larger aggregates have used imaging systems to characterize their distributions, usually using a single
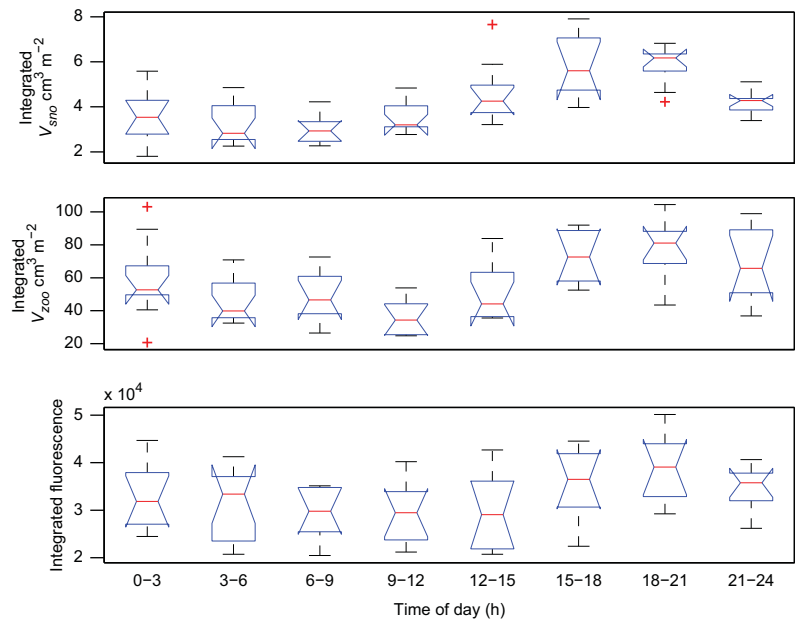
Fig. 12. Daily cycles for th07_4. Top: vertically integrated total s-particle abundances as time of day; middle: vertically integrated total z-particle concentrations; bottom: vertically integrated fluorescence concentrations. Integrated values were grouped into 3 h intervals. Data for each group are represented as box plots, as discussed for Fig. 4. In this case, the amounts of s-particles from 15 to 21 h appear to be significantly greater than those between midnight and noon. Similarly, the z-particle concentrations at 18–21 h are significantly above those for 9-12 h. The differences in integrated fluorescence are not evident. There were between 9 and 12 profiles for each group. (Calculated using the boxplot.m function in Matlab.)
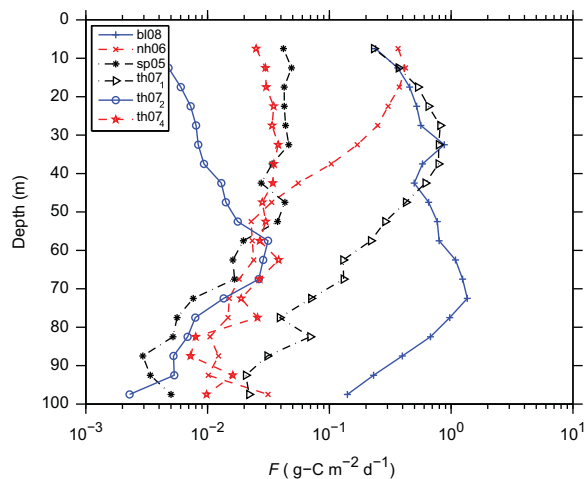

Fig. 13. Particle flux associated with the mean s-particle distribution, as a function of depth for multiple deployments. Fluxes were not calculated for sp_07 because of the lack of a good estimate for f.

number to describe particle concentration. For example, Stemmann et al. (2000) used their imaging Underwater Video Profiler (UVP) to count particles larger than 150 µm between 90–1000 m depth in the Mediterranean Sea. They found that larger particles were more abundant at night and argued that fecal pellet production by vertically migrating zooplankton could be responsible for the diel signal. Walsh et al. (1995) also observed a diel pattern in particle abundance. McCave et al. (2001) observed a subsurface maximum in particle number and volume at 50 m but could not see evidence of a strong diel cycle. We observed a diel signal in two of our eight deployments.

Lampitt et al. (1993b) observed aggregates with an imaging system in the NE Atlantic and calculated volumetric concentrations as high as 400 ppm at about 50 m. They measured

vertical particle fluxes at 50 m, observing fluxes between 100 and 704 mg dry wt $m^{-2}\,d^{-1}$.

MacIntyre et al. (1995) collected 33 profiles of particles off Southern California in April and May 1990–1992 using imaging techniques. They expressed their results as the number concentration of particles with $d_{od} > 0.05$ cm. Their typical peak particle abundance in a vertical profile was $50-60\,L^{-1}$; the typical peak mean particle volume was 0.4–5 mm^3, equivalent to $d_{esd} = 0.1-0.2$ cm. These values are similar to what we observed (Fig. 6). As noted above, for the equivalent $d_{od} = 0.12$ mm, we observed similar concentrations, with $N = 19-254\,L^{-1}$ at th07_1 .

All single measures of particle distributions have their weaknesses. The number of particles larger than a given diameter, equivalent to using N for a fixed d, is extremely sensitive to small errors in d because of the rapid variation of N as a function of d (e.g., Fig. 6). This change in N results from the presence of many more small particles than large ones. Interpreting particle concentrations using spectra provides a means of accounting for size effects. Another measure, the total particle volume (V_{tot}), is sensitive to the presence or absence of rare large particles.

4.3. Particle formation and distributions: coagulation

The strongest correlation of particles with the environment that we observed was between V_{sep} and the fluorescence signal, which was proportional to the chlorophyll concentration. In addition, the maximum particle concentrations were rarely shallower than the fluorescence maxima. These distributions are consistent with s-particles being aggregates, algae being important sources for them, and their sinking after formation.

The mean particle size increased with depth for our deployments. This observation is also consistent with coagulation models, in which particles continue to aggregate and become larger as they fall (Burd and Jackson, 2009). Larger particles tend to fall faster (e.g., Asper, 1987; Alldredge and Gotschalk, 1989; Pilskaln et al., 1998). Thus, the tendency of particles to form

aggregates accelerates the vertical movement of matter downward.

Goldthwait and Alldredge (2006) surveyed observations about diel periodicity in particle abundance, finding evidence for a decrease at night (Graham et al., 2000) and for a decrease during the day (Stemmann et al., 2000), with both attributed to interactions with zooplankton. Goldthwait and Alldredge (2006) made three sets of observations, finding evidence for decreases during the day one time, decreases during the night a second time, and no evidence for diel cycling a third time. Particles are such a part of the planktonic system that multiple factors can affect them.

MacIntyre et al. (1995) observed a similar decrease in particle abundance with increasing depth. They noted that some increase in turbulence could increase aggregation rates, but that too much turbulence could tear aggregates apart. They speculated that the decrease was the result of disaggregation of falling aggregates caused by enhanced turbulence deeper in the pycnocline. If this were so, we would expect to see an accumulation of phytoplankton and a decrease in particle size in the region of disaggregation. We do not see that in our fluorescence signals. Furthermore, there was no correlation between the density gradient, as denoted by N_{BV}^2, and any of the particle metrics. If aggregates were being torn apart by increased turbulence in the pycnocline, there should have been a negative correlation between N_{BV}^2 and particle volume.

4.4. Relating particle size distributions and fluxes

A prediction of particle flux using the particle size spectrum assumes that these particles do settle as a function of size. Multiple lines of evidence support the assumption that particles in the size range that we observed do settle. For example, Abramson et al. (2010) reported a correspondence between the composition of particles larger than 81 μm and material collected in sediment traps and argued that their distribution could be used to infer fluxes. The s-particles used for the flux calculations had $d_{od} > 2000$ μm and were well within the range of their settling particles. Divers have observed particles larger than 1 mm settling within the euphotic zone (Alldredge and Gotschalk, 1989). Lastly, the size distributions of particles have been used successfully to estimate fluxes observed sediment trap fluxes (Jackson et al., 2005; Guidi et al., 2008; Iversen et al., 2010). Because the actual relationships between particle diameter and settling velocity vary spatially and temporally, the fluxes calculated here are best considered as relative. However, when considering the relative changes of flux at a given location and time, they do provide strong information about vertical distribution of processes that alter the flux.

Material in particle traps located in the upper 100 m is typically composed of algal-derived aggregates, non-descript aggregates, and fecal pellets (e.g., Goldthwait and Alldredge, 2006; Wexels Riser et al., 2001). Off Greenland and in the Barents Sea, fecal pellets typically composing only 10–35% of the flux (Juul-Pedersen et al., 2006; Wexels Riser et al., 2001). Most of the flux was aggregated material.

Analyses of material caught in sub-euphotic zone sediment traps frequently have found that fecal pellet-derived material dominates the collected mass (e.g., Abramson et al., 2010; Ebersbach and Trull, 2008). These results from sediment trap studies are not directly comparable to our study, as the shallowest trap in a given study is usually considerable deeper than the upper 50–100 m studied here. Ranges for the shallowest traps for some of these studies include 100–200 m (Ebersbach and Trull, 2008), 150 m (Buesseler et al., 2008), and 117–313 m (Abramson et al., 2010). Our results imply very sharp decreases right at the bottom of the surface layer, here much shallower than 100 m. The difference between particle flux at the base of the actual euphotic zone and the geochemist's working border at 100 m has been discussed by Buesseler and Boyd (2009).

4.5. Fate of particles and zooplankton feeding

The fact that there must be intense activity at the base of the euphotic zone has been observed and commented on previously. Lampitt et al. (1993b) observed a sharp drop in particle concentration at the base of the mixed layer. They suggested that animal feeding on particles there could be responsible for the sharp change. They further noted that "sharp vertical gradients in marine snow distributions and high sinking rates imply short time-scales of production and loss."

Olli et al. (2001) made high spatial resolution measurements of particle flux off the NW coast of Spain in which the POC flux dropped in half between 50 and 70 m depth. Similarly, Wassmann et al. (2003) show profiles of vertical flux in the Barents Sea in which the vertical flux again dropped in half over relatively short distances, there between 60 and 90 m. Particularly striking were the sizes of the fluxes, about 1 g C m^{-2} d^{-1} in the Barents Sea and 160 mg C m^{-2} d^{-1} off Spain, and the associated consumption. Wassmann et al. (2003) reached the same conclusion about the necessary importance, noting the strong attenuation of the vertical flux at the base of the euphotic zone. Wexels Riser et al. (2001) coined the phrase "retention filter" to describe the phenomenon.

Iversen et al. (2010) measured particle size distributions in the Atlantic Ocean off northwest Africa down to a depth of 2500 m. From these distributions, they estimated the decrease in particle flux as functions of depth and particle size. Iversen et al. (2010) found that the relative rate at which particle flux decreased with depth $(1/nv\,\partial nv/\partial z)$ was constant across their particle size classes. They noted that this is a characteristic of flux feeding, rather than zooplankton filter-feeding or microbial degradation. Stemmann et al. (2004) used a more elaborate model of particle transformations to reach a similar conclusion about the relative importance of flux feeding below 100 m in the Mediterranean.

If consumption of falling particulate matter is important, there should be chemical traces of the process. Vertical profiles of ammonium concentrations frequently show peak concentrations below the euphotic zone. For example, Johnson et al. (2007) measured ammonia profiles during the North Atlantic bloom. Ten of their 15 profiles had maxima between 50 and 100 m. Plant et al. (2009) presented an ammonium profile off Monterey Bay, California, which had maximum concentrations of about 200 nM at 50 m depth, compared to background values of 5–10 nM.

In addition, there is geochemical evidence that this is a region of intense recycling. Buesseler et al. (2008) measured ^{234}Th concentrations through the euphotic zone and below, finding an excess of ^{234}Th at the base of the euphotic zone. They interpreted this as indicating the base of the euphotic zone is a region where falling particles bring ^{234}Th from above, leaving it behind when they are consumed and remineralized by animals there.

The formation of aggregates and subsequent enhanced sinking of algal mass separates the regions of primary production and its consumption. Zooplankton are frequently (Napp et al., 1988; Herman, 1984), but not always (Herman, 1983), found in the region of the particle concentration maximum, not at the shallower production maximum. For this separation between production and feeding to be sustainable, there must be a movement of material from the site of production to the site of feeding. While clearly not the only sites of zooplankton feeding, the deeper regions around the base of the euphotic zone, with the aggregates

found there, are important regions of feeding by zooplankton and microbes.

Aggregates provide previously unappreciated feeding opportunities for zooplankters, by allowing flux feeding, the use of chemical and hydromechanical cues, and mining (Shanks and Walters, 1997; Dagg, 1993; Jackson, 1993; Jackson and Kiørboe, 2004). There are zooplankton that are known to associate with marine snow (e.g., Shanks and Edmondson, 1990; Shanks and Walters, 1997; Green and Dagg, 1997). Other species, such as the copepod *Neocalanus cristatus* (Dagg, 1993; Liu et al., 2008) and the amphipod *Themisto compressa* (Lampitt et al., 1993b), have morphologies and distributions suggesting that they specialize on consuming falling aggregates at the base of the euphotic zone and deeper. Their abilities to consume picoplankton $< 1\,\mu m$ despite their inabilities to capture isolated particles $< 5\,\mu m$ provides further evidence that they feed on aggregates (Dagg, 1993; Lampitt et al., 1993b). Animals, without such specialized morphologies, including *Euphausia pacifica*, are known to feed on aggregates, even in the presence of high concentrations of dispersed cells (Dilling and Brzezinski, 2004).

Kiørboe et al. (1998) and Tiselius and Kiørboe (1998) described a similar situation in the Benguela Current, where diatoms in high concentration aggregated and fell. Despite their enhanced fall velocities, the diatom aggregates never reached the bottom because they were consumed by *Noctiluca scintillans* present in large concentrations at the base of the thermocline. This is a particularly unambiguous example of flux feeding (Jackson, 1993) controlling the vertical transport of organic matter at the base of the euphotic zone.

For a flux feeder, eating where the food supply is largest is a good strategy. Eating at the base of the euphotic zone puts the animals where the food supply is greatest, and before it is consumed by another animal. So, it makes sense that the region be the site of intense activity. Feeding at the base of the euphotic zone has the advantage of taking the zooplankters away from the intense mortality due to visual predation in the surface high light environment to a region where the lower irradiance lessens effectiveness of visual predation (e.g., Aksnes and Giske, 1993).

Feeding on the flux is clearly not the best strategy for all animals at all times. As can be seen comparing Figs. 9 and 13, the relative range of peak particle volume, about 0.8–5 ppm, was less than a factor of ten, compared to the almost hundred-fold range in peak particle flux as a result of changes in average particle sizes. It is interesting that the range in fluxes at 100 m is also much smaller.

4.6. Implications

The sharp decrease that we observe in particle concentrations with depth is consistent with previous observations of particle concentrations, particle fluxes, and chemical and isotopic signatures. Our results also agree with ideas about flux from the euphotic zone and the role of animals as gatekeepers.

However, interpreting the results solely in terms of the movement of production from the euphotic zone to the mesopelagic hides the importance of this flux within the euphotic zone. As shown in Fig. 13, the flux increases gradually with depth before dropping off at the particle maximum. Thus, this flux represents a transfer of organic matter within the euphotic zone and a spatial separation of production and consumption that is mediated by the formation and accelerated sinking of larger particles. Thus, the same particle properties that drive the mesopelagic are important in the euphotic zone. In addition, feeding on particles at the base of the particle maximum is an additional means for heterotrophs to find and consume particles other than just filter-feeding.

The canonical view of upper ocean biogeochemistry has been organized around relatively rigid separation between the euphotic zone and the underlying mesopelagic. Phytoplankton production has been characterized by the *f*-ratio and new production, which described the relative settling loss from the system (Eppley and Peterson, 1979). It was matched by a geochemical view in which the particle flux started at 100 m (Martin et al., 1987). This view separates processes (production, flux) which transcend boundaries between the euphotic and mesopelagic zones.

Buesseler and Boyd (2009) have started a reassessment of how we think about the sub-euphotic zone processes, emphasizing the importance of zooplankton transformations between the bottom of the euphotic zone and the conventional geochemical boundary at 100 m. They did not include aggregation in their analysis, nor did they include the euphotic zone. We argue that the same processes that move material out of the euphotic zone also move them within the surface layer as well. Furthermore, the conceptual idea that there is a distinct boundary at the base of the euphotic zone is an oversimplification. Because the largest decrease in particle concentration and flux is near the boundary of the euphotic and mesopelagic zones, we argue that this region is characterized by feeding below the particle maximum and is a zone of intense biological activity.

Steinberg et al. (2008) studied the vertical distribution of zooplankton at the VERTIGO particle flux study sites. They were able to assign their animals to different functional feeding types, including different types of particle feeders. Their near-surface vertical resolution, 50 m, was too small to tease out the relationships discussed here.

The spatial separation of primary production and consumption affects our understanding of the spatial nature of the euphotic zone. For those regions in which aggregate formation and settling are important processes in the movement of nutrients, it provides a spatial separation of primary and secondary production that is rarely included in plankton models. The movement of material downward even within the euphotic zone makes the details of the upward flux of nutrients crucial to the functioning of theses systems.

Flux feeding associated with the particle maximum may also change our view of zooplankton competition. The maximum resource of a flux feeder occurs in one location. If there is no primary production below the particle maximum, then the flux below it is determined by the number of feeders above. The maximum feeding rate is at the flux maximum. However, being shallower exposes animals to a greater risk of mortality from visual predators as a result of the higher irradiance there (Aksnes and Giske, 1993).

Dominant processes change through the water column. Within the euphotic zone, aggregation produces faster settling particles (e.g., Jackson, 1990; Hill, 1992). Aggregation changes to zooplankton feeding and fecal pellet processing. Much is occurring at the base of the euphotic zone. Any mismatch between animals and flux will allow material to pass through (e.g., Jackson and Burd, 2002).

To understand and, hence, predict interactions of particles, zooplankton, and flux, we will need to have better models and more precise measurements focussed in the transition region between euphotic and mesopelagic zones.

4.7. Final thoughts

The picture that emerges of particles in the euphotic zone is that multiple processes determine the fate of primary production. Particle coagulation and settling combine with zooplankton

grazing to remove and redistribute primary production. The amount of material that leaves the euphotic zone, entering the mesopelagic, depends in part on the zooplankton that serve as gatekeepers at the base of the particle maximum layer.

Better resolution of organism distributions in conjunction with observations on particles and their properties is crucial to our understanding and prediction of the vertical flux and hence ocean biogeochemistry. The ability of autonomous particle counters, such as the SOLOPC, to sample hourly with high resolution in a region where sediment traps are used only sparingly provides an important tool for the study of particle dynamics in the ocean.

Acknowledgements

References

Abramson, L., Lee, C., Liu, Z., Wakeham, S.G., Szlosek, J., 2010. Exchange between suspended and sinking particles in the northwest Mediterranean as inferred from the organic composition of in situ pump and sediment trap samples. Limnol. Oceanogr. 55, 725–737.

Aksnes, D.L., Giske, J., 1993. A theoretical model of aquatic visual feeding. Ecol. Model. 67, 233–250.

Alldredge, A.L., Gotschalk, C.C., 1988. Direct observations of the mass flocculation of diatom blooms: characteristics, settling velocities and formation of diatom aggregates. Deep-Sea Res. 36, 159–171.

Alldredge, A.L., Gotschalk, C.C., 1989. In situ settling behavior of marine snow. Limnol. Oceanogr. 33, 339–351.

Asper, V.L., 1987. Measuring the flux and sinking speed of marine snow aggregates. Deep-Sea Res. 34, 1–17.

Buesseler, K.O., Andres, J.E., Pike, S.M., Charette, M.A., Goldson, L.E., Brzezinski, M.A., Lance, V.P., 2005. Particle export during the Southern Ocean Iron Experiment (SOFeX). Limnol. Oceanogr. 50, 311–327.

Buesseler, K.O., Antia, A.N., Chen, M., Fowler, S.W., Gardner, W.D., Gustafsson, O., Harada, K., 2007. An assessment of the use of sediment traps for estimating upper ocean particle fluxes. J. Mar. Res. 65, 345–416.

Buesseler, K.O., Boyd, P.W., 2009. Shedding light on processes that control particle export and flux atttenuation in the twilight zone of the open ocean. Limnol. Oceanogr. 54, 1210–1232.

Buesseler, K.O., Lamborg, C., Cai, P., Escoube, R., Johnson, R., Pike, S., Masque, P., McGillicuddy, D., Verdeny, E., 2008. Particle fluxes associated with mesoscale eddies in the Sargasso Sea. Deep-Sea Res. II 55, 1426–1444.

Burd, A.B., Jackson, G.A., 2009. Particle aggregation. Ann. Rev. Mar. Sci. 1, 65–90.

Checkley, D.M., Barth, J.A., 2009. Patterns and processes in the California Current System. Prog. Oceanogr. 83, 49–94.

Checkley, D.M., Davis, R.E., Herman, A.W., Jackson, G.A., Beanlands, B., Regier, L.A., 2008. Assessing plankton and other particles in situ with the SOLOPC. Limnol. Oceanogr. 53, 2123–2136.

Dagg, M., 1993. Sinking particles as a possible source of nutrition for the large calanoid copepod Neocalanus cristatus in the subarctic Pacific Ocean. Deep-Sea Res. I 40, 1431–1445.

Dilling, L., Brzezinski, M.A., 2004. Quantifying marine snow as a food choice for zooplankton using stable silicon isotope tracers. J. Plankt. Res. 26, 1105–1114.

Ebersbach, F., Trull, T.W., 2008. Sinking particle properties from polyacrylamide gels during the KErguelen Ocean and Plateau compared Study (KEOPS): zooplankton control of carbon export in an area of persistent natural iron inputs in the Southern Ocean. Limnol. Oceanogr. 53, 212–224.

Eppley, R.W., Peterson, B.J., 1979. Particulate organic matter flux and planktonic new production in the deep ocean. Nature 282, 677–680.

Gehlen, M., Bopp, L., Emprin, N., Aumont, O., Heinze, C., Ragueneau, O., 2006. Reconciling surface ocean productivity, export fluxes and sediment composition in a global biogeochemical ocean model. Biogeosci. 3, 521–537.

Goldthwait, S.A., Alldredge, A.L., 2006. An investigation of diel synchronicity between water column marine snow concentration and the flux of organic matter in the Santa Barbara Channel, California. Deep-Sea Res. I 53, 485–505.

Gonzalez-Quiros, R., Checkley Jr., D.M., 2006. Occurrence of fragile particles inferred from optical plankton counters used in situ and to analyze net samples collected simultaneously. J. Geophys. Res. 111. doi:10.1029/2005JC003084.

Graham, W.M., MacIntyre, S., Alldredge, A.L., 2000. Diel variations of marine snow concentration in surface waters and implications for particle flux in the sea. Deep-Sea Res. I 47, 367–395.

Green, E.P., Dagg, M.J., 1997. Mesozooplankton associations with medium to large marine snow aggregates in the northern Gulf of Mexico. J. Plankt. Res. 19, 435–447.

Guidi, L., Jackson, G.A., Stemmann, L., Miquel, J.C., Picheral, M., Gorsky, G., 2008. Particle size distribution and flux in the mesopelagic: a close relationship. Deep Sea Res. I. 55, 1364–1374.

Guidi, L., Stemmann, L., Legendre, L., Picheral, M., Prieur, L., Gorsky, G., 2007. Vertical distribution of aggregates ($> 110\,\mu m$) and mesoscale activity in the northeastern atlantic: effects on the deep vertical export of surface carbon. Limnol. Oceanogr. 52, 7–18.

Herman, A.W., 1983. Vertical distribution patterns of copepods, chlorophyll and production in the northeastern Baffin Bay. Limnol. Oceanogr. 28, 709–719.

Herman, A.W., 1984. Vertical copepod aggregations and interactions with chlorophyll and production on the Peru shelf. Cont. Shelf Res. 3, 131–146.

Herman, A.W., Beanlands, B., Phillips, E.F., 2004. The next generation of Optical Plankton Counter: the Laser-OPC. J. Plankt. Res. 26, 1135–1145.

Hill, P.S., 1992. Reconciling aggregation theory with observed vertical fluxes following phytoplankton blooms. J. Geophys. Res. 97, 2295–2308.

Iversen, M.H., Nowald, N., Ploug, H., Jackson, G.A., Fischer, G., 2010. High resolution profiles of vertical particulate organic matter export off Cape Blanc., Mauritania: degradation processes and ballasting effects. Deep-Sea Res. I 57, 771–784.

Jackson, G.A., 1990. A model of the formation of marine algal flocs by physical coagulation processes. Deep-Sea Res. 37, 1197–1211.

Jackson, G.A., 1993. Flux feeding as a mechanism for zooplankton grazing and its implications for vertical particulate flux. Limnol. Oceanogr. 38, 1328–1331.

Jackson, G.A., 1995. Comparing observed changes in particle size spectra with those predicted using coagulation theory. Deep-Sea Res. II 42, 159–184.

Jackson, G.A., Burd, A.B., 2002. A model for the distribution of particle flux in the mid-water column controlled by subsurface biotic interactions. Deep-Sea Res. II 49, 193–217.

Jackson, G.A., Kiørboe, T., 2004. Zooplankton use of chemodetection to find and eat particles. Mar. Ecol. Prog. Ser. 269, 153–162.

Jackson, G.A., Maffione, R., Costello, D.K., Alldredge, A.L., Logan, B.E., Dam, H.G., 1997. Particle size spectra between 1 m and 1 cm at Monterey Bay determined using multiple instruments. Deep-Sea Res. 44, 1739–1767.

Jackson, G.A., Waite, A.M., Boyd, P.W., 2005. Role of algal aggregation in vertical carbon export during SOIREE and in other low biomass environments. Geophys. Res. Lett. 32, L13607. doi:10.1029/2005GL023180.

Johnson, M., Sanders, R., Avgoustidi, V., Lucas, M., Brown, L., Hansell, D., Moore, M., Gibb, S., Liss, P., Jickells, T., 2007. Ammonium accumulation during a silicate-limited diatom bloom indicates the potential for ammonia emission events. Mar. Chem. 106, 63–75.

Juul-Pedersen, T., Nielsen, T.G., Michel, C., Møller, E.F., Tiselius, P., Thor, P., Olesen, M., Selander, E., Gooding, S., 2006. Sedimentation following the spring bloom in Disko Bay, West Greenland, with special emphasis on the role of copepods. Mar. Ecol. Prog. Ser. 314, 239–255.

Kiørboe, T., Tiselius, P., Mitchell-Innes, B., Hansen, J.L.S., Visser, A.W., Mari, X., 1998. Intensive aggregate formation with low vertical flux during an upwelling-induced diatom bloom. Limnol Oceanogr 43, 104–116.

Lampitt, R.S., Hillier, W.R., Challenor, P.G., 1993a. Seasonal and diel variation in the open ocean concentration of marine snow aggregates. Nature 362, 737–739.

Lampitt, R.S., Wishner, K.F., Turley, C.M., Angel, M.V., 1993b. Marine snow studies in the Northeast Atlantic Ocean: distribution, composition and role as a food source for migrating plankton. Mar. Biol. 116, 689–702.

Landry, M.R., Ohman, M.D., Goericke, R., Stuekl, M.R., Tsyrklevich, K., 2009. Lagrangian studies of phytoplankton growth and grazing relationships in a coastal upwelling ecosystem off Southern California. Prog. Oceanogr. 83, 208–216.

Liu, H., Dagg, M.J., Napp, J.M., Sato, R., 2008. Mesozooplankton grazing in the coastal Gulf of Alaska: Neocalanus spp vs. other mesozooplankton. ICES J. Mar. Sci. 65, 351–360.

MacIntyre, S., Alldredge, A.L., Gotshalk, C.C., 1995. Accumulation of marine snow at density discontinuities in the water column. Limnol. Oceanogr. 40, 449–468.

Martin, J.H., Knauer, G.A., Karl, D.M., Broenkow, W.W., 1987. VERTEX: carbon cycling in the northeast Pacific. Deep-Sea Res. 34, 267–285.

McCave, I.N., Hall, I.R., Antia, A.N., Chou, L., Dehairs, F., Lampitt, R.S., 2001. Distribution, composition and flux of particulate material over the European margin at 47°–50° N. Deep-Sea Res. II 48, 3107–3139.

Mullin, M.M., Sloan, P.R., Eppley, R.W., 1966. Relationship between carbon content, cell volume, and area in phytoplankton. Limnol. Oceanogr. 11, 307–311.

Napp, J.M., Brooks, E.R., Matrai, P., Mullin, M.M., 1988. Vertical distribution of marine particles and grazers. II. Relation of grazer distribution to food quality and quantity. Mar. Ecol. Prog. Ser. 50, 59–72.

Olli, K., Wexels Riser, C., Wassman, P., Ratkova, T., Arshkevich, E., 2001. Vertical export of biogenic matter, particulate nutrinets, and mesozooplankton faecal pellets. Prog. Oceanogr. 51, 443–466.

Pilskaln, C.H., Lehmann, C., Paduan, J.B., Silver, M.W., 1998. Spatial and temporal dynamics in marine aggregate abundance, sinking rate and flux: Monterey Bay, central California. Deep-Sea Res. II 45, 1803–1837.

Plant, J.N., Johnson, K.S., Needoba, J.A., Coletti, L.J., 2009. NH4-Digiscan: an in situ and laboratory ammonium analyzer for estuarine, coastal, and shelf waters. Limnol. Oceanogr. Meth. 7, 144–156.

Shanks, A.L., Edmondson, E.W., 1990. The vertical flux of metazoans (holoplankton, meiofauna, and larval invertebrates) due to their association with marine snow. Limnol. Oceanogr. 32, 455–463.

Shanks, A.L., Walters, K., 1997. Holoplankton, meroplankton, and meiofauna associated with marine snow. Mar. Ecol. Prog. Ser. 156, 75–86.

Steinberg, D.K., VanMooy, B.A.S., Buesseler, K.O., Boyd, P.W., Kobari, T., Karl, D.M., 2008. Bacterial vs. zooplankton control of sinking particle flux in the ocean's twilight zone. Limnol. Oceanogr. 53, 1327–1338.

Stemmann, L., Picheral, M., Gorsky, G., 2000. Diel variation in the vertical distribution of particulate matter (> 0.15 mm) in the NW Mediterranean Sea investigated with the underwater video profiler. Deep-Sea Res. I 47, 505–531.

Stemmann, L., Jackson, G.A., Gorsky, G., 2004. A vertical model of particle size distributions and fluxes in the midwater column that includes biological and physical processes. II. Application to a three year survey in the NW Mediterranean Sea. Deep-Sea Res. 51, 885–908.

Tiselius, P., Kiørboe, T., 1998. Colonization of diatom aggregates by dinoflagellate *Noctiluca scintillans*. Limnol. Oceanogr. 43, 154–159.

Trent, A.D., Shanks, A.L., Silver, M.W., 1978. In-situ and laboratory measurements on macroscopic aggregates in Monterey Bay, California. Limnol. Oceanogr. 23, 626–635.

Walsh, I.D., Gardner, W.D., 1992. A comparison of aggregate profiles with sediment fluxes. Deep-Sea Res. 39, 1817–1834.

Walsh, I.D., Chung, S.P., Richardson, M.J., Gardner, W.D., 1995. The diel cycle in the integrated particle load in the equatorial Pacific: a comparison with primary production. Deep-Sea Res. II 42, 465–479.

Wassmann, P., Olli, K., Riser, C.W., Svensen, C., 2003. Ecosystem function, biodiversity and vertical flux regulation in the twilight zone. In: Wefer, G., Lamy, F., Mantoura, F. (Eds.), Marine Science Frontiers for Europe. Springer-Verlag, pp. 279–287.

Wexels Riser, C., Wassman, P., Olli, K., Arashkevich, E., 2001. Production, retention, and export of zooplankton faecal pellets on and off the Iberian shelf, north-west Spain. Prog. Oceanogr. 51, 423–441.